Chapter 1

Microwave Fast Sintering of Double Perovskite Ceramic Materials

Penchal Reddy Matli, Adel Mohamed Amer Mohamed and Ramakrishna Reddy Rajuru

Additional information is available at the end of the chapter

http://dx.doi.org/10.5772/61026

Abstract

The book chapter mainly deals with the microwave sintering of high quality crystals of La_2MMnO_6 (M = Ni or Co) ceramics. Double perovskite La_2MMnO_6 (M = Ni or Co) ceramics with average particle size of ~65 nm were manufactured using microwave sintering at 90°C for 10 min in N_2 atmosphere for the first time. The morphology, structure, composition, and magnetic properties of the prepared compacts were characterized using X-ray diffraction (XRD), scanning electron microscopy (SEM), transmission electron microscopy (TEM), energy-dispersive X-ray spectroscopy (EDX), infrared spectroscopy (IR and FTIR), and physical properties measurement system (PPMS). The corresponding dielectric property was tested in the frequency range of 1 kHz–1 MHz and in the temperature range of 300–600 K, and the ceramics exhibited a relaxation-like dielectric behavior.

Keywords: ceramics, microwave sintering, microstructures, XPS, multiferroic properties

1. Introduction

Microwave sintering (MWS) is emerging and an innovative sintering technology for processing of ceramic materials and is commonly related with volumetric and uniform heating. MWS is one of the exciting new fields in material science with vast potential for preparation of novel and/or nanostructured ceramics/materials. Microwave heating has some important benefits

over normal heating for ceramic processing, including reduced processing time, higher energy efficiency, selective and controlled heating, environmental friendliness, and improved product uniformity and yields. Microwave processing of materials is a relatively new technology that can be used in wide range of different materials such as ceramics, ferroelectrics, oxides, metals, and composites [1–10].

The effect of microwave radiation on the processing of several ceramic materials such as magnetic materials, superconducting materials, dielectric materials, metals, polymers, ceramics, and composite materials offers numerous benefits over conventional heating techniques. These benefits include time and energy savings, volumetric and uniform heating, considerably reduced processing time and temperature, improved product yield, fine microstructures, improved mechanical properties, lower environmental impact, reduction in manufacturing cost, and synthesis of new materials [11].

Microwave sintering has developed in recent years as a promising technology for faster, cheapest and most environmental-friendly processing of a wide variety of materials, which are regarded as significant advantages over conventional sintering procedures. Microwave radiation/heating for sintering of ceramic constituents has recently appeared as a newly motivated scientific approach [5].

Microwave sintering approach has unique advantages over conventional sintering methods in many respects. The essential difference in the conventional and microwave sintering processes is in the heating mechanism (Figure 1). In microwave heating, the materials themselves absorb microwave energy and then transform it into heat within the sample volume and sintering can be completed in shorter times. In microwave sintering, the heat is generated internally within the test sample due to the rapid oscillation of dipoles at microwave frequencies [12]. The contribution of diffusion from external sources is lesser. The internal and volumetric heating makes the sintering rapidly and uniformly. The heat generated through conventional heating is generally transferred to the sample via radiation, conduction, and convention [13]. This process takes longer duration for sintering the materials and causes some of the constituents to evaporate. This may lead to modify the desired stoichiometry and grain.

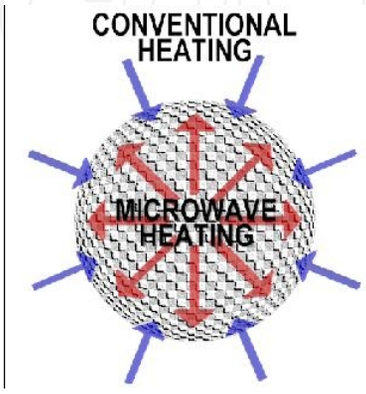

Figure 1. Comparison of heating mechanism in microwave and conventional sintering methods.

In contrast, microwave energy is transferred directly to the material through molecular interaction with an electromagnetic field. Microwave heating is more effective than conventional methods in terms of the usage of energy, produces higher temperature homogeneity, and is considerably faster than conventional heat sources. In the last 8 years, we have successfully sintered various ferrites/ferroelectrics, oxides, ceramics, mullite fiber, composites, and even powdered metals to full density using microwave processing [4, 5, 14–16].

Due to the energy efficient nature of microwave heating, there is a great opportunity for the application of microwaves to process metal based materials to couple the many gains of microwave heating. Recently, microwaves energy has been successfully used in different composites, metal, ceramics, melting of metals and metal ores, joining or brazing of metals, and heat treatment of metals [17].

The microwave energy is highly versatile in its application in the field of communication, and it still dominates almost all communications in space and mobile or cordless phone technology involves microwave frequencies. However, other than this communication, microwave energy has found its use for a variety of applications including rubber products industry, food processing, wood/paper/textile/ceramic drying, pharmaceuticals, polymers, printing materials, and biomedical fields over the past 50 years. These applications involve low temperature (<500°C) utilization of microwaves. The high temperature (> 800°C) applications of microwaves are a rather recent phenomenon.

Many researchers have reported that microwave heating is relatively faster than the conventional heating processes. This faster speed is manifested as a reduction in the densification time of ceramic powder compacts, often allied to lower sintering temperatures [7]. Generally, the synthesis kinetics and sintering materials are apparently upgraded by two or three orders of magnitude or even more when conventional heating is switched for microwave heating [18].

1.1. Interaction of microwaves with ceramic materials: theoretical aspects

Microwaves are electromagnetic waves with the electromagnetic radiations in the frequency band of 300 MHz to 300 GHz, and their corresponding wavelength between 1 m and 1 mm can be used successfully to heat many ceramic materials. Since most of the microwave band is used for communication purpose, the Federal Communications Commission has allocated only very few specific frequencies for industrial, scientific, and medical applications. A major portion of these microwave used in the communication sector and only certain frequencies, viz., 0.915, 2.45, 5.85, and 21.2 GHz, are chosen for medical and industrial applications. Among these allowed frequencies, 2.45 GHz is the most common microwave frequency used for industrial and scientific applications. The interaction and heating generation of ceramics under microwave field depends on the dielectric, magnetic, and conductive loss of the material and temperature dependent parameters.

The ability of a material to be heated in microwave field depends on its dielectric properties, characterized by the dielectric complex constant ε^*:

$$\varepsilon^* = \varepsilon' - j\varepsilon'' \tag{1}$$

Dielectric permittivity ε' represents the material capacity to store electromagnetic energy and loss factor ε'' to dissipate it.

The dielectric constant of a material varies with its temperature, frequency, and composition. The power P absorbed in the material is proportional to the loss factor ε'', the frequency f [Hz], and the electric field intensity E [V/m]:

$$P = 2\Pi f \varepsilon^0 \varepsilon'' E^2 \tag{2}$$

(or)

$$P = 55.63 \times 10^{-2} f \varepsilon' \tan\delta E^2 \tag{3}$$

where the dielectric loss angle (loss tangent) is

$$\tan\delta = \frac{\varepsilon''}{\varepsilon'}, \tag{4}$$

Eq. (3) shows that for a fixed value of electric field (E), the power in microwave absorbed in the material mass is proportional to the frequency (f) (which is practically 2.45 GHz), the dielectric permittivity (ε'), and loss factor (ε'') (through the loss tangent tan δ), which vary with the materials temperature and humidity in their turn.

The diffusion of electromagnetic power into the absorber is characterized by skin depth (D) and expressed as

$$D = \left(\pi f \mu \sigma\right)^{-1/2} \tag{5}$$

where μ and σ are magnetic permeability and electrical conductivity and f is the frequency, respectively.

The effective penetration depth decreases with increase in frequency which in turn causes less heating. Hence, a suitable combination of parameters in Eqs. (2) and (4) is required for achieving optimum coupling. It can be inferred from this discussion that low dielectric loss materials take longer time and high dielectric loss materials take shorter duration in the microwave sintering.

On a microscopic scale, the phenomenon of dielectric heating is the effect of impurity dipolar relaxation in the microwave frequency region. When the vacancy jumps around the impurity

ion to align its dipole moment with the electric field the internal friction of the rapidly oscillating dipole cause a homogeneous (volumetric) heating. Where the maximum absorption of microwave energy at the frequency or temperature at which the loss factor (tan δ) attains its maximum. This is equivalent to an elastic relaxation resulting in damping of mechanical vibrations in solids.

The efficiency of the microwave dielectric heating is dependent on the ability of a specific material (powder, solvent, or reagent or anything else) to absorb microwave energy and convert it into heat. The heat is generated by the electric component of the electromagnetic field through two main mechanisms, i.e., dipolar polarization and ionic contribution [19]. According to the electromagnetism, the effect of a material upon heat transfer rates is often expressed as

$$\frac{\Delta T}{t} = \frac{0.56 \times 10^{-10} \varepsilon''_{eff} f E^2}{\rho C_p} \tag{6}$$

where ε''_{eff} is the effective relative dielectric loss factor, f is the frequency of microwave, E is the magnetic fields of microwave within the material, ρ is the mass density of the sample, and C_P is the isotonic specific heat capacity [19]. In this case, the energy efficiency can easily reach 80–90% utilization and higher than the conventional heating methods [20, 21]. However, the essential nature of the interaction between microwaves and reactant molecules during the preparation of materials is fairly uncertain and speculative.

1.2. Benefits of microwave sintering comparison to conventional sintering method

In recent years, microwave sintering has shown significant advantages against conventional sintering for the synthesis of ceramic materials. Microwave sintering has attained worldwide attention due to its major advantages against conventional sintering methods, especially in ceramic materials.

Microwave sintering can significantly shorten the sintering time leading to consume much lower energy than conventional sintering.

There are major potential and real advantages using microwave energy for material processing over conventional heating. These include the following:

- Time and energy savings
- Reduced processing time and temperature
- Rapid, volumetric, and selective heating
- Fine microstructures
- Improved physical and functional properties
- Lower environmental impact

- Controllable electric field distribution

1.3. Applications of microwave sintering of ceramic materials

Now microwave processing has been found that this technique can also be applied as efficiently and effectively to powdered metals as to many ceramics. Finally, The MWS operational expenses are less than 50–80% to the conventional sintering techniques. The MWS technique works 20 times faster than the conventional sintering method and takes only few minutes for processing than the conventional ones (takes hours).

1.4. Brief introduction of multiferroics

Multiferroic materials exhibits both ferroelectric and magnetic in nature and have much attracted research interest due to their potential application in multistate data storage and electric field controlled spintronics. Among all the studies related to the materials, transition metal oxides with perovskite structure are noteworthy [22, 26].

Multiferroic materials with double-perovskite structure $\left(AA^{'}BB^{'}O_6\right)$ are solid solutions of two perovskites: (ABO_3) and $\left(A^{'}B^{'}O_3\right)$. In $\left(AA^{'}BB^{'}O_6\right)$, A and A′ represent alkaline rare earth cations (La, Y, and Ce), while B and B′ are transition metal cations (Ni and Co). If A and A′ represent the same chemical element, the double perovskite has the general formula $\left(A_2BB^{'}O_6\right)$ and the crystal structure of $A_2BB^{'}O_6$ -type perovskite, as shown in Figure 2. Alkali-earth and lanthanide (smaller ion) ions are alone usually occupied in the A site [27, 28]. If the A ion is too small, the common expected distortions are cation displacement with BO_6 and octahedral ones [29].

The most representative $\left(A_2BB^{'}O_6\right)$ ferromagnetic double perovskites are La_2NiMnO_6 [30–33], La_2CoMnO_6 [5, 34, 35], La_2BMnO_6 [36–48], and La_2FeMnO_6 [41, 42].

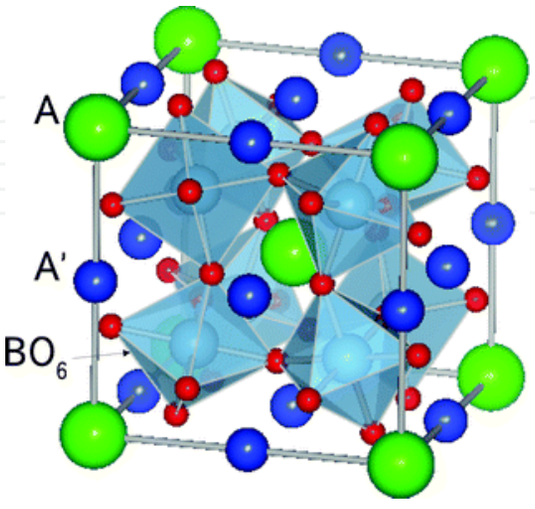

Figure 2. Crystal structure of $A_2BB'O_6$ type perovskite. The spheres at A and A′-site are for La and at B′-site are for Ni, Co. The network of corner-sharing BO_6 octahedra isare shown where oxygen atoms are in the corner of octahedra.

La_2NiMnO_6 (LNMO) has gained more attention as a rare example of a single-material platform with multiple functions, such as ferromagnetic (FM) semiconducting properties up to room temperature, magnetocapacitance, and magnetoresistance effects. The spin lattice coupling characteristics of LNMO exhibits a larger magnetodielectric (MD) effect close to room temperature. It has been well documented that the spins, electric charge, and dielectric functions in LNMO are turned by magnetic or electric fields. LNMO is considered as an FM semiconductor and shows Curie transition temperature (T_c) very close to room temperature. This property in LNMO makes the Ni^{2+} and Mn^4 ions ordered and occupied the centers of BO_6 (corner shared) and $B'O_6$ structures respectively. This arrangement leads to the distribution of ideal double perovskite.

LNMO's structural system, La_2CoMnO_6 (LCMO), possesses an FM T_c ~225 K with an insulating behavior. The magnetic properties of the LCMO are strongly depending on the cation ordering, valences, defects, and synthetic conditions.

Among them, double perovskite La_2NiMnO_6 (LNMO) and La_2CoMnO_6 (LCMO) ceramics are attractive due to their impressive properties and potential on industrial applications [30–33, 42, 43]. LNMO is a ferromagnetic semiconductor with high critical temperature of T_c~280 K, which may be used in commercial solid-state thermoelectric (Peltier) coolers [42]. LCMO is also a ferromagnetic semiconductor with critical temperature of T_c ~230 K [35–37]. Several crystal structures have been identified, and it is confirmed that the ferromagnetic semiconductors LNMO and LCMO with high T_c are $P^2_{1/n}$ monoclinic structure, in which octahedra with Ni (or Co) and Mn centers alternately stacking along (111). Recent reports indicate LNMO and LCMO have considerable magnetodielectric effects at room temperature, which is very useful for future electronic device [29, 35, 44, 45].

The double perovskites La_2MMnO_6 (M = Co and Ni) are one of the most commonly occurring and important in all of materials science because they can exhibit novel magnetic, electric, and optical properties [28–44]. La_2MMnO_6 crystallizes in a double perovskite structure with rock salt configuration of MO_6 and MnO_6 octahedra. The ordering of M^{2+} and Mn^{4+} gives rise to 180° super exchange interactions based on Goodenough–Kanamori rules and consequently high ferromagnetic Curie transition temperature [43].

It is familiar that the properties of double perovskite compounds are strongly influenced by the materials composition and microstructure, which are sensitive to the preparation technique employed for their synthesis [46]. Various synthesis techniques such as sol–gel [30, 32, 35], coprecipitation [31], solid-state reaction method [33, 34], microwave sintering process [5], molten-salt synthetic process [26, 27] sol-gel autocombustion [41], and chemical solution deposition method [47] have been reported in the preparation of double perovskite compounds. Each of the techniques has its own merits and limitations. For instance, conventional sintering is a simple and relatively cheap method with a long holding time (several hours), formation of lots of undesirable intermetallic compounds, and nonhomogeneous pore-size distribution. In the recent years, microwave sintering has emerged as a new sintering method for ceramics, semiconductors, metals, and composites.

Microwave sintering (MWS) technique has gained a lot of significance in recent times for materials (metals, composites, ceramics/nanoparticles) synthesis and sintering mainly because of its intrinsic advantages [5] such as rapid heating rates, reduced processing times, substantial energy savings novel and improved properties, finer microstructures, and being environmentally more clean. Therefore, it is viewed as one of the most advanced sintering techniques in material processing [5, 48] and improved physical and mechanical properties [7]. It has been shown that microwave sintering technique may provide enhanced densification in sintering of metal, oxides and non-oxide ceramics [5, 48, 49, 50].

However, to the best of our knowledge in the open literature, there have been only a few reports so far on the fabrication of double perovskite nanoparticles by microwave sintering approach [5, 51]. The purpose of the current chapter will focus on fabrication of the double perovskite La_2MMnO_6 (M = Ni, Co) ceramics and in order to further improve their magnetic and dielectric properties for practical spintronic applications through microwave sintering approach.

2. Experimental procedure

2.1. Materials

All the chemical reagents were of analytical pure grade (99.99%) and used without further purification. The versatile chemical coprecipitation–microwave sintering process [15] employed in present investigation is two-step process which consists of coprecipitation method is the first step of synthesis followed by microwave sintering in second half of experiment. High-purity $La(NO_3)_3.5H_2O$ (Merck), $Ni(NO_3)_2.6H_2O$ (Sigma-Aldrich), $Co(NO_3)_2.6H_2O$ (Sigma-Aldrich), and $Mn(NO_3)_3.4H_2O$ (Sigma-Aldrich) were used as starting materials. In a typical experimental process, the high purity stoichiometric amounts of $La(NO_3)_3.5H_2O$, $Ni/CO(NO_3)_2.6H_2O$, and $Mn(NO_3)_3.4H_2O$ were dissolved in appropriate amounts of deionized water and magnetically stared vigorously for 2 h at 80°C. The ammonia solution was used until to get 8.5 PH value. The stirring will continue for about 30 min, and the suspension was ball milled for about 24 h with ethanol as a milling media. The reactants were to be mixed well and then dried at 80°C in a cabinet drier for 24 h to obtain precursor powder sample. Then the powder was subjected to microwave sintering under uniform heating to get dense ceramics.

2.2. Microwave sintering setup

Microwave processing systems usually consist of a microwave source, for generation of microwaves, a circulator, an applicator to deliver the power to the load, and systems to control the heating and the experimental diagram of the microwave sintering set up used is shown in Figure 3. Most applicators are multimode, where different field patterns are excited simultaneously.

Further, In order to achieve pure double perovskite phases, the precursor samples were put into 2.45 GHz, 6 kW continuously adjustable microwave equipment (HAMiLab-HV3, Syno-Therm), the maximum operating temperature up to 1400°C, and 0.5–3 kW. The multimode

microwave furnace consists of a cubical stainless steel chamber with a side of 30 cm. Two magnetrons (microwave source), each with a maximum rated power of 1100 watts, are situated opposite to each other. A box made of alumina, zirconia, and silica mixed cardboard is used as a thermal insulator. The material is positioned in the center of box and is surrounded by silicon carbide (susceptor) plates.

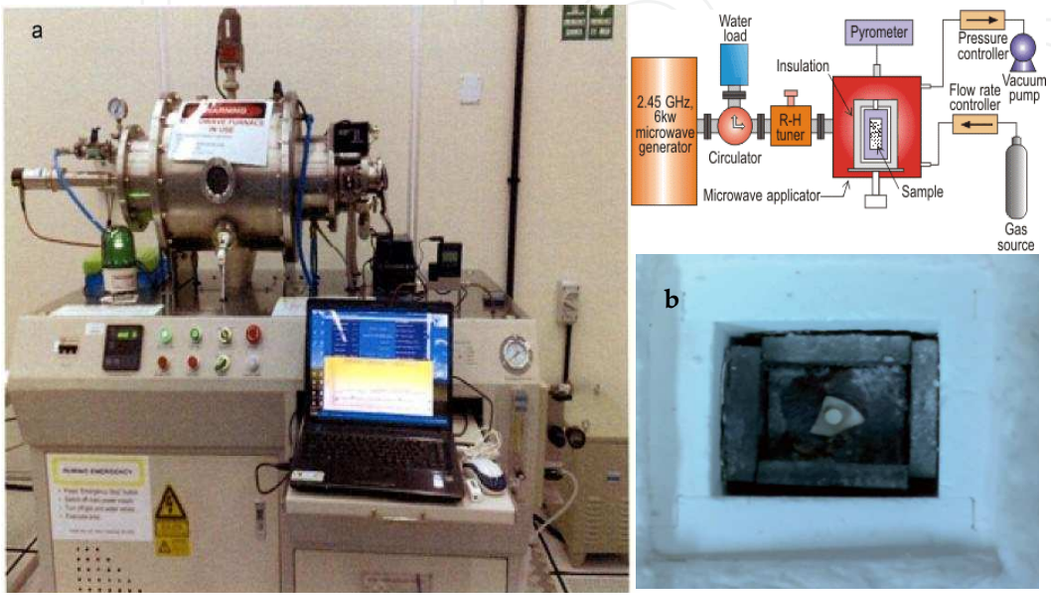

Figure 3. Experimental setup of multimode microwave furnace [3] (a) and Ssusceptor (b).

During the sintering process, the microwave sintering chamber was filled with high purity nitrogen gas flow (99.999%). An adjustable programmed electrical control system was used to deliver the required energy to the sample. The employed heating chamber was made up with stainless steel double walled tubular cavity with water-cooled facility, and the maintained processing temperature is about 1400°C. A high purity quartz crystal cylinder arrangement is available inside the chamber, where the samples were loaded for processing; the temperature of the sample was measured using infrared pyrometer during the MW sintering. The SiC plates surrounded in the crucible were served as susceptors and provide initial heating to be compact disc samples. Once the materials received absorb sufficient MW heat including the core and will get uniform heating. The secondary purpose of SiC is to maintain the surface temperature. The crucible was positioned at the center of the furnace so it provides strong MW radiation. The green compacted disks for heated at 900°C for 10 min in atmospheric N_2 ambient temperature and heating rate of 20°C/min is maintained by varying magnetron power between 1000 and 2500 W followed by normal frequency cooling.

2.3. Characterization and property measurements of La_2MMnO6 (M = Ni, Co) ceramics

The crystal structure of the microwave sintered products was characterized by X-ray diffraction (XRD) using a Shimadzu X-ray diffractometer with Cu-K_α radiation 2θ range of 20 to 80°. Raman spectra were carried out on an RM-1000 micro-Raman spectrometer with the 514.53

nm line of an argon laser under ambient conditions. The composition, morphology, and microstructures of the products were characterized by transmission electron microscope (TEM FEI Tecnai F20 microscope, Japan) and field emission scanning electron microscope (FESEM, Hitachi S-4800, Japan) equipped with an energy-dispersive X-ray spectrometer (EDS). Fourier transform infrared spectroscopy (FTIR) was performed on a Nicolet 5700 spectrometer in the wave number range of 400–4000 cm^{-1}. The spectroscopic grade KBr pellets were used for collecting the spectra with a resolution of 4 cm^{-1} performing 32 scans. X-ray photoelectron spectroscopy (XPS) was performed on an ESCA-UK XPS system with an Mg K_{α} excitation source (hν = 1486.6 eV), where the binding energies were referenced to the C1s peak at 284.6 eV of the surface adventitious carbon. The magnetic properties were measured using a physical property measurement system (PPMS-9, Quantum Design, Inc., San Diego, CA, USA) at room temperature under a maximum field of 20 kOe. Silver paste was applied on both sides of the pellet for the electrical measurements. The variation of dielectric constant and dielectric loss as a function of frequency at room temperature and as a function of temperature at different frequencies was measured using computer interfaced HIOKI 3532-50 LCR-HITESTER.

3. Microwave-sintering of engineered double perovskite ceramic materials

3.1. Crystal structure of La_2MMnO6 (M = Ni, Co) ceramics

The phase structure of the microwave sintered LNMO and LCMO nanoparticles was characterized by X-ray diffraction (XRD). As shown in Figure 4, no extra reflection peaks other than those of pure perovskite phase are detected, indicating the high purity of nanoparticles can be obtained in 10 min by this microwave sintering approach, which confirms the formation of single phase compositions of LNMO and LCMO double perovskites [30].

The crystallite size was calculated from XRD patterns using the Debye–Scherrer formula [7], described by the Eq. (7):

$$D = \frac{0.94 \times \lambda}{\beta_{1/2} \times \cos\theta} \tag{7}$$

where D = crystallite size, λ = radiation wavelength (1.5405 Å), $\beta_{1/2}$ = half-width of diffraction profile, and θ = diffraction angle.

The average crystal size was found to be 23 nm for LNMO and 28 nm for LCMO, which are 2–3 times smaller than the particle/grain sizes measured by TEM as shown in below section.

Raman spectroscopy is one of the most important tools to attain the information about the structure of the samples. The Raman spectra of microwave sintered LNMO and LCMO ceramics are shown in Figure 5. The Raman spectra display two characteristics peaks at around 514, 653 cm^{-1} for LNMO and 488, 670 cm^{-1} for LCMO ceramics, corresponding to the well-documented A band and B band, respectively. Martín–Carron et al. have assign the two peaks

http://dx.doi.org/10.5772/61026

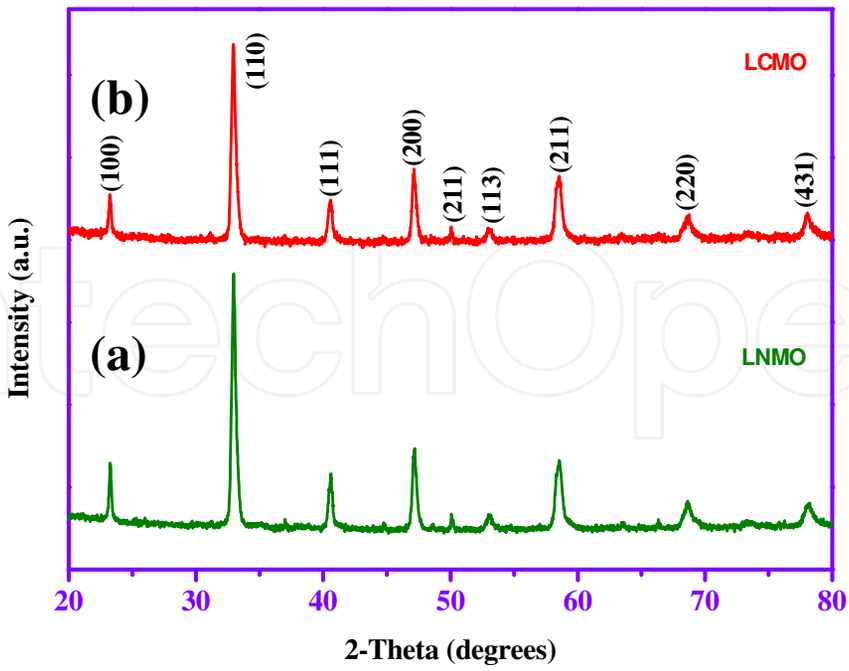

Figure 4. XRD patterns of the microwave sintered (a) LNMO and (b) LCMO ceramics.

to the A_g antisymmetric stretching (or Jahn–Teller stretching mode) and B_g symmetric stretching vibrations of the MnO_6 octahedra, respectively [34–36, 52–54]. It is well known that the A_g band is usually assigned to antisymmetric stretching (or Jahn–Teller stretching mode), while the B_g band distributed to symmetric stretching vibrations. A noticeable difference is seen between our LNMO/LCMO ceramics and the bulk sample: the A_g and B_g peaks for the nanoparticles shift to higher binding energy, 13 and 25 cm^{-1}, respectively, when compared to the bulk crystal. The shifting may occur due to surface strain of the crystal structure [55].

The microstructure and morphology of microwave sintered LNMO and LCMO ceramics were investigated by FESEM and TEM techniques. Typical SEM images of La_2MMnO_6 (M = Ni, Co) nanoparticles are shown in Figure 6, the average grain size is about 52 nm and 58 nm for La_2NiMnO_6 and La_2CoMnO_6, respectively. The grain size of La_2CoMnO_6 is bigger than that of La_2NiMnO_6, which obeys the rule that relatively large ionic radius id benefit to the diffusion in the microwave sintering process.

From the morphologies of both samples, the grains seem to be homogeneous and form a group of cluster phenomenon. The perovskite material has better microwave absorption capability [5, 51] and leads to fine grain growth during the sintering process.

The EDX spectra (inset of 6a and 6b) and their corresponding tables confirm the presence of the constituent elements (La, Ni, Co, Mn, and O), the composition being nearly the same as that of stoichiometric La_2NiMnO_6 and La_2CoMnO_6, respectively.

As shown in Figures 7a and 7b, transmission electron microscopy (TEM) was applied for all samples to determine particle size and confirmed that the particle sizes are about 53 ± 12 and 60 ± 15 nm for LNMO and LCMO, respectively, which agrees good agreement with the SEM

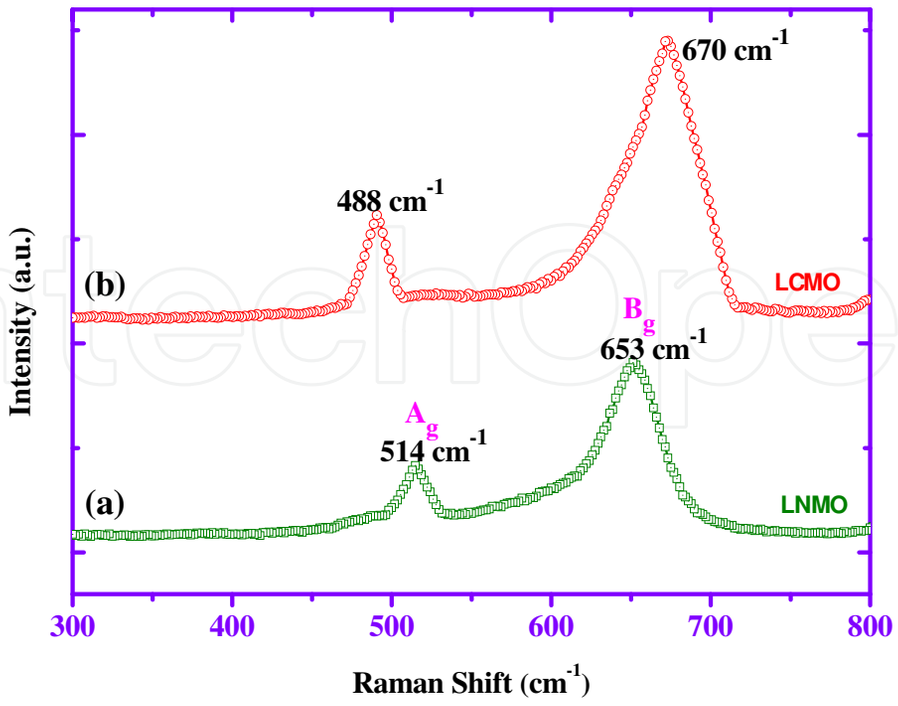

Figure 5. Raman of the microwave sintered (a) LNMO and (b) LCMO ceramics.

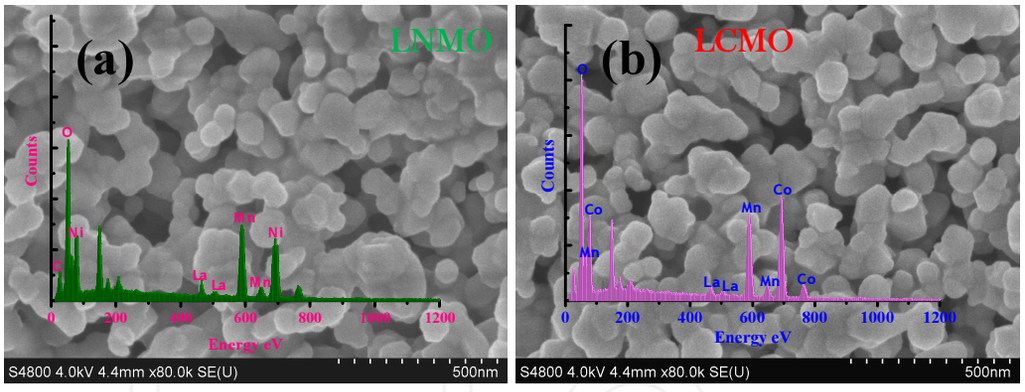

• OK• 23.45• 57.12•	• OK• 25.15• 55.55•
• LaL• 04.12• 01.23•	• LaL• 04.25• 01.08•
• NiK• 45.95• 27.01•	• CoK• 46.75• 28.03•
• MnK• 23.67• 15.63•	• MnK• 23.85• 15.34•
• Matrix• Correction• ZAF•	• Matrix• Correction• ZAF•

Figure 6. FESEM images, EDX spectra (inset) and elemental data of the microwave sintered (a) LNMO and (b) LCMO ceramics.

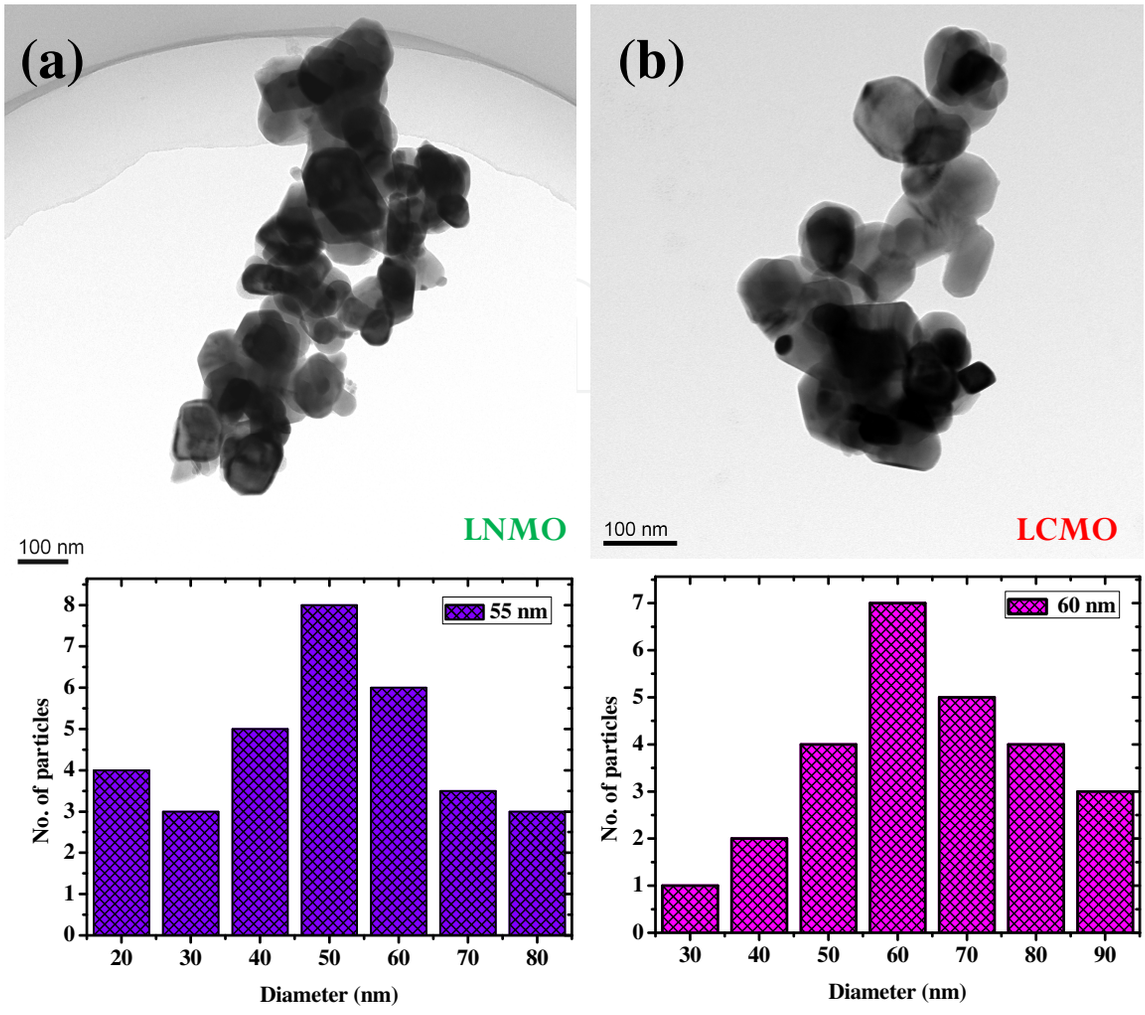

Figure 7. TEM images and particle size distributions of the microwave sintered (a) LNMO and (b) LCMO ceramics.

results. From the TEM micrograph, nanosized grains with quasi spherical shape can be observed.

The formation mechanism of the perovskite type structure in the microwave sintered LNMO and LCMO ceramics is further supported by FT-IR spectrum shown in Figure 8. The FTIR spectrum is used to characterize the phase composition and purity of the prepared samples. The intense peak around 3423 cm^{-1} is referring to the stretching vibration of hydroxyl group. In addition, the bands at about 1629 cm^{-1} can be ascribed to the asymmetric COO^- stretching vibrations. The bands at 1450 and 1357 cm^{-1} attributed to the asymmetric stretching of CO_3^{2-}. The intensive absorption band observed at 597cm^{-1} can be assigned to Fe–O stretching vibrations formed by the octahedral MnO_6 group.

The chemical states of elements of Ni, Mn in LNMO, and Co, Mn in LCMO ceramics was further investigated by X-ray photoelectron spectroscopy. The XPS core level spectra of Ni 2p, Co 2p, and Mn 2p of La_2MMnO_6 (M = Ni, Co) are presented in Figure 9. A Ni $2P_{3/2}$ signal was observed at 851.3 eV along with a satellite peak at 858.5 eV. Another peak was noticed at 869.5 eV and

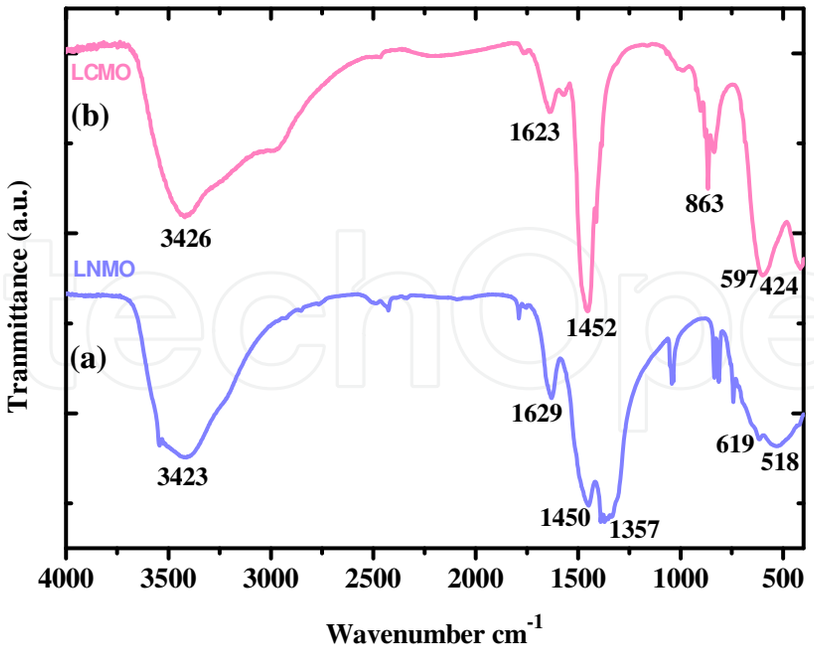

Figure 8. FTIR of the microwave sintered (a) LNMO and (b) LCMO ceramics.

ascribed to the Ni $2P_{1/2}$ level. Auger electron peak of Ni of [Figure 9a] explains the presence of +2 oxidation state of the nickel in LNMO ceramics. The Mn $2p_{3/2}$ peak of LNMO is at 638.4 eV, while the same Mn $2p_{3/2}$ peak is at 641.5 eV for Mn_2O_3 [56]. In the spectrum of Co2p (Figure 6c), the peaks of Co $2p_{3/2}$ and Co $2p_{1/2}$ states were located at 777.3 and 782.7 eV, respectively [57]. The Mn $2p_{3/2}$ peak of LCMO shown in Figures 6 b and 6d is found at 637.6 eV, close to that in Mn_2O_3 [56].

3.1.1. Magnetic analysis of La_2MMnO_6 (M = Ni, Co) ceramics

The magnetization characteristics were measure both as a function of applied magnetic field at fixed temperatures and as a function of temperature at fixed fields. The room temperature hysteresis loops of the microwave sintered La_2MMnO_6 (M = Ni, Co) ceramics were measured using physical property measurement system (PPMS). The magnetization curves, as shown in Figures 10a and 10c, display relatively high saturation magnetization. The magnetic saturation (M_s) values of LNMO and LCMO are 42.9 and 65.4 emu/g, respectively, which is lower their theoretical values of 47.5 and 71.21 emu/g reported in the literature [40]. One can note that MWS products saturation magnetization was higher than for the conventionally sintering products [36], indicating that MWS method is efficient to fabricated high quality double perovskite material.

The frequency dependence of saturation magnetization hysteresis curves was recorded at room temperature for the LNMO ceramics as shown in Figure 10a. A hysteresis loop has been observed at 5 K with a coercive field of ~282 Oe and remnant magnetization of ~7.7 emu/g, which show that the LNMO sample exhibit typical ferromagnetic behavior. Figure 10c shows the variation of magnetization as a function of magnetic field for LCMO ceramics. A hysteresis

http://dx.doi.org/10.5772/61026

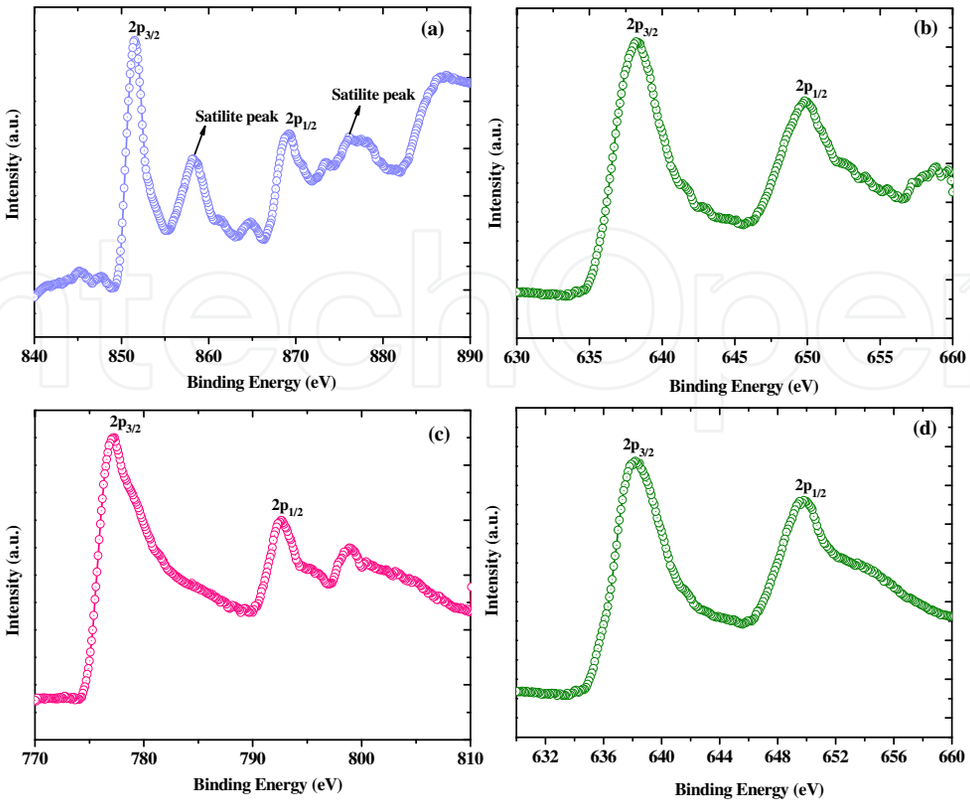

Figure 9. High-resolution XPS spectra's of (a) Ni 2p peaks, (b) Mn 2p peaks for LNMO and (c) Co 2p peaks, (d) Mn 2p peaks for LCMO ceramics.

loop has been observed at 5 K with a coercive field of ~972 Oe and remnant magnetization of ~8.14 emu/g, which show that the LCMO sample exhibit typical super paramagnetic behavior. Apart from the magnetic characteristics presented here, detailed examination is in progress and the extensive and expected results will be reported elsewhere shortly.

Figures 10b and 10d show the temperature dependence of magnetization measurements for LNMO and LCMO under an applied field was carried out by field-cooled (FC) and zero-field-cooled (ZFC) processes at an applied magnetic field of 100 Oe in the temperature range of 5–400 K. For the LNMO, It could be observed from ZFC as well as FC magnetization that the material shows two ferromagnetic transitions around 270 K and 240 K, which is reliable with the presence of two phases as showed by the X-ray diffraction studies. As the ferromagnetic transition temperature in the pure monoclinic phase is found to be near 255 K, we attribute the ferromagnetic transition at 240 K to the rhombohedral phase. FC magnetization reaches a maximum value of ~3.2 emu/g at 5 K. The magnetic transition at ~255 K indicates the onset of FE long-range ordering, very close to the magnetic transition temperature (T_c = ~280 K) reported earlier in the literature [41]. It is pertinent to maintain that there is a divergence between ZFC and FC magnetization curves below 220 K for the LCMO. Noticeable difference has also been observed in the case of low field ZFC and FC magnetization for LNMO particles. These LCMO nanoparticles possess a single magnetic transition at about 225 K under 100 Oe

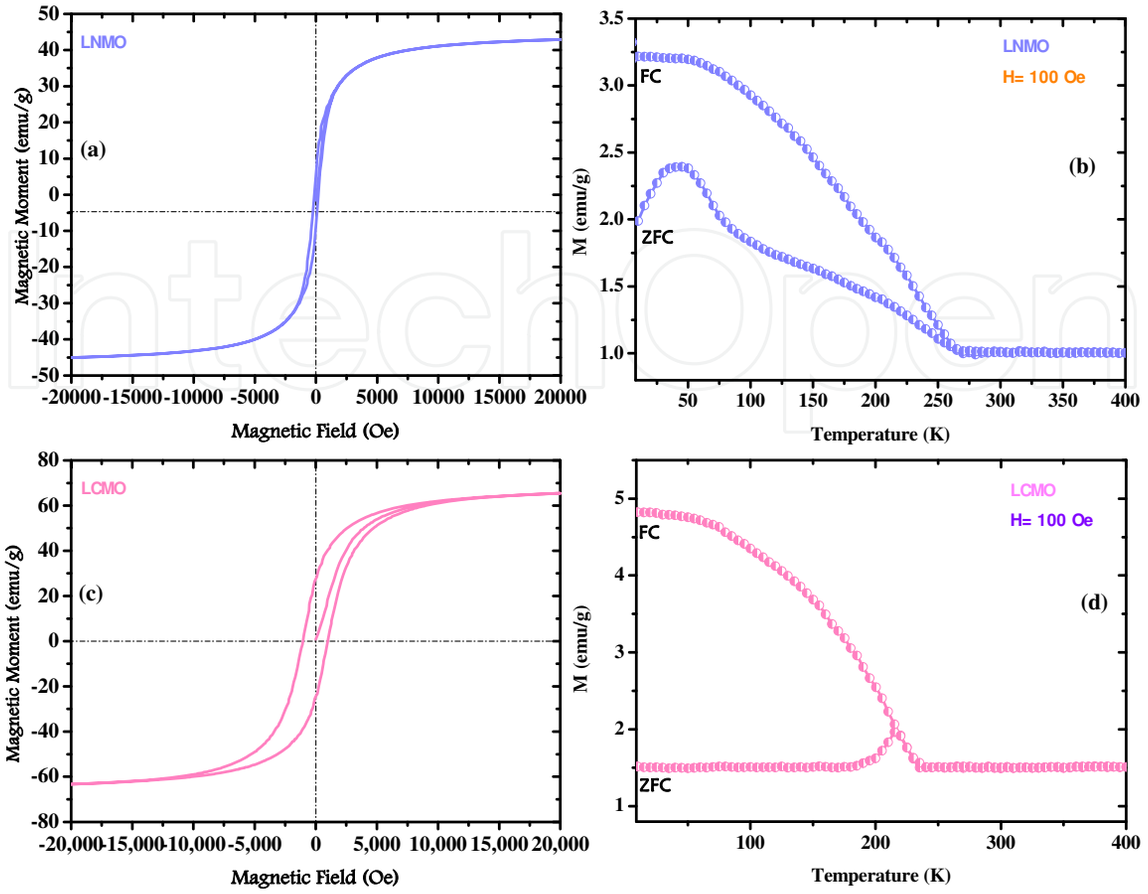

Figure 10. Magnetic field dependent magnetization data at 5 K (a and c), zZero-Ffield-Ccooled (ZFC) and Ffield-Ccooled (FC) magnetization as a function of temperature (b and d) the microwave sintered LNMO and LCMO ceramics.

field. This observation is very close to the behavior of bulk LCMO ceramics [58]. The maximum FC magnetization is noticed about 4.8 emu/g at 5 K.

3.2. Dielectric properties of La_2MMnO_6 (M = Ni, Co) ceramics

The temperature variation of dielectric constant (ε') and loss tangent (tan δ) at different frequencies ranging from 1 kHz to 1 MHz for the microwave sintered La_2MMnO_6 (M = Ni, Co) ceramics is shown in Figures 11a–11d. Noticeably, the dielectric constant (ε') decreases significantly with increasing frequency. An interesting Maxwell–Wager relaxation [59]-type dielectric behavior (at high dielectric constant) has been noticed around 450 K in these materials and also strong dispersion in the relaxation spectra. The dielectric constant is gradually increased first along with the increase in temperature and attains significant growth at a critical temperature. The critical temperature value shifts toward higher side as and when the measuring frequency increases. These features indicate the thermally activated process [59]. This phenomenon has been most widely described in various earlier reports [24, 59–61].

Such dielectric performance could be attributed to the cationic disorder prompted by the exchange of B sites [62]. In the present systems, Ni^{3+}/Co^{3+} and Mn^{4+} ions instantly exist in B sites, which results in two kinds of BO_6 octahedra in the structure of La_2MMnO_6. Therefore, the ion disorder in the unit cell should be one of the causes for this behavior.

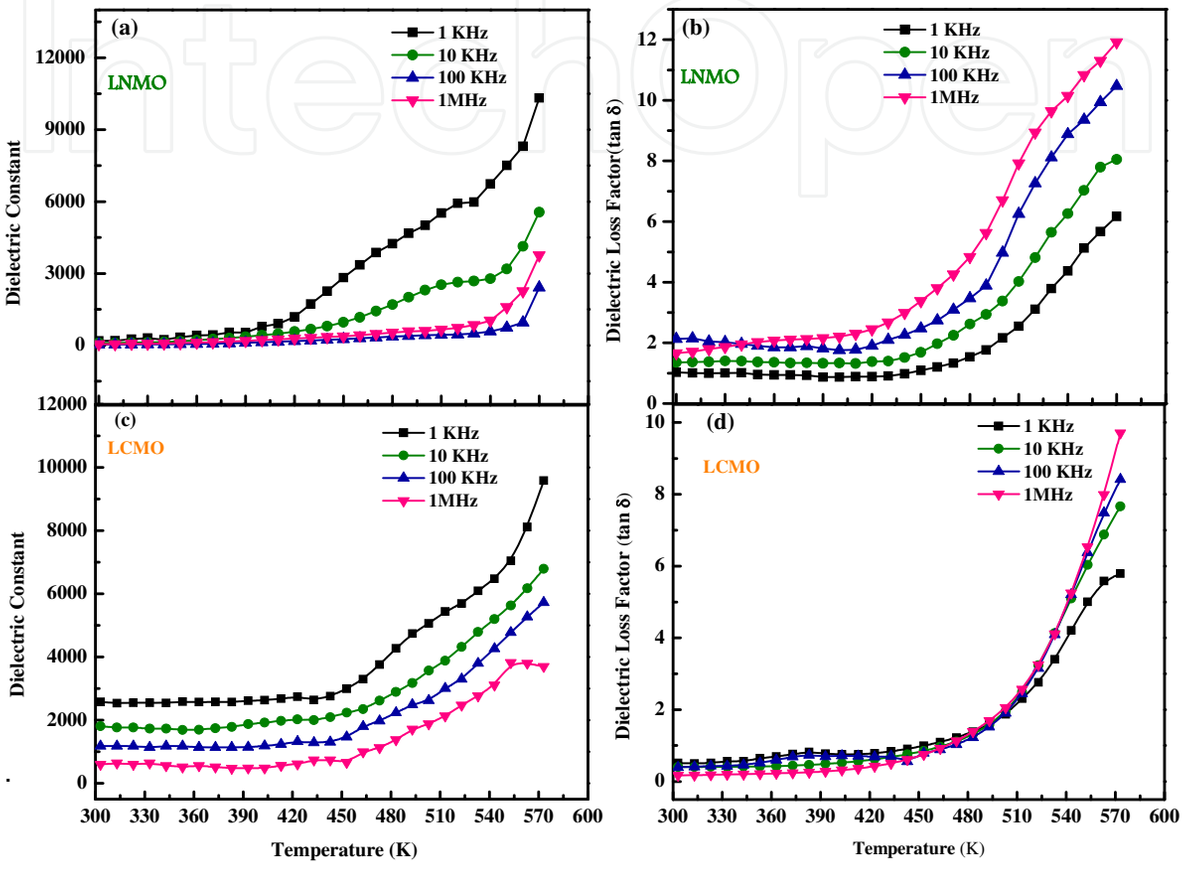

Figure 11. Temperature dependence of dielectric constant and dielectric loss of the microwave sintered (a & b) LNMO and (c & d) LCMO ceramics at various frequencies.

Figures 12a and 12b show the dielectric constant (ε') as a function of frequency of LNMO and LCMO ceramics at different temperatures. It can be observed that the dielectric constant of both ceramics decreases as frequency increases. The decrease in the dielectric constant with increase in frequency can be explained by the behavior on the basis of electron happing from Fe^{2+} to Fe^{3+} ions or on basis of decrease in polarization with the increase in frequency. Polarization of a dielectric material is the quantity of the contributions of ionic, electronic, dipolar, and interfacial polarizations [63]. At low frequencies, polarization mechanism is keenly observed at low frequencies to the time varying electric fields. As the frequency of the electric field increases, different polarization contributions are filter out under leads to the decrement in net polarization under dielectric constant. Similar behavior has also been reported by different investigators earlier in the literature [60, 64]. The physical, magnetic, and dielectric properties of LMNO and LCMO are summarized in Table 1.

Parameters	LNMO	LCMO
d_{XRD} (nm)	23	28
d_{TEM} (nm)	53	60
A_g (cm^{-1})	514	653
B_g (cm^{-1})	488	670
M_s (emu/g)	42.9	65.4
M_r (emu/g)	7.7	8.14
H_c (Oe)	272	972
T_N (K)	225	240
DC (1 MHz)	161	19.7
DL (1 MHz)	1.235	0.172

Table 1. Physical and multiferroic characteristics of the microwave sintered LNMO and LCMO nanoparticles

4. Conclusions and scope of the future work

In this chapter, double perovskite La_2MMnO_6 (M = Ni, Co) ceramics were successfully prepared using microwave sintering technique. The microwave sintering approach shows obviously better promise over the conventional heating method, in terms of higher efficiency of heating, significantly shorter reaction time, smaller and more regular size, and stronger magnetization of the products. IR, XRD, and SEM-EDX analysis confirmed the formation of single phase for La_2MMnO_6 (M = Ni, Co) double perovskites. XPS gives information about the oxidation state and chemical stoichiometric composition of the perovskite samples. The oxidation states of transition metals are Ni^{2+} and Mn^{4+} in the samples. The variation with temperature of a sample's magnetization can give Neel temperatures of about 240 K for LNMO and 225 K for LCMO. Multiferroic properties of microwave sintered ceramics were found to be higher than that of the values reported for conventionally sintered samples. Microwave processing greatly reduced the processing time and improved the magnetic and dielectric properties, which hinted its superiority over conventional processing. Hence, the microwave sintering technique is more facile approach for the preparation of the industrially important perovskite-type ceramics.

Furthermore, one can study the correlation between different magnetic and electric order parameter for this material, to use as a potential candidate for multiferroics. The magnetization dynamics can be studied to know the spin–spin interactions. Low temperature dielectric spectroscopy can also be studied to know whether this material undergoes any transition or not and if so what is the inside story of this transition and much more work can be done related to this material.

Author details

Penchal Reddy Matli[1*], Adel Mohamed Amer Mohamed[1,2] and Ramakrishna Reddy Rajuru[3]

*Address all correspondence to: drlpenchal@gmail.com

1 Center for Advanced Materials, Qatar University, Doha, Qatar

2 Department of Metallurgical and Materials Engineering, Faculty of Petroleum and Mining Engineering, Suez University, Suez, Egypt

3 Department of Physics, Sri Krishnadevaraya University, Anantapur, India

References

[1] Vasylkiv O, Demirskyi D, Sakka Y, Ragulya A, Borodianska H. Densification kinetics of nanocrystalline zirconia powder using microwave and spark plasma sintering—a comparative study. Journal of Nanoscience and Nanotechnology 2012;12: 4577–82.

[2] Demirskyi D, Borodianska H, Grasso S, Sakka Y, Vasylkiv O. Microstructure evolution during field-assisted sintering of zirconia spheres. Scripta Materialia 2011;65: 683–6.

[3] Shannigrahi SR, Pramoda KP, Nugroho FAA. Synthesis and characterizations of microwave sintered ferrite powders and their composite films for practical applications. Journal of Magnetism and Magnetic Materials 2012;324: 140–145.

[4] Penchal Reddy M, Madhuri W, Balakrishnaiah G, Ramamanohar Reddy N, Siva Kumar KV, Murthy VRK, Ramakrishna Reddy, R. Microwave sintering of iron deficient Ni–Cu–Zn ferrites for multilayer chip inductors. Current Applied Physics 2011;11: 191–8.

[5] Penchal Reddy M, Zhou XB, Jing L, Huang Q. Microwave sintering, characterization and magnetic properties of doubleperovskiteLa_2CoMnO_6 nanoparticles. Material Letters 2014;132: 55–8.

[6] Demirskyi D, Agrawal D, Ragulya A. Neck growth kinetics during microwave sintering of copper. Scripta Materialia 2010;62: 552–5.

[7] Roy R, Agrawal D, Cheng J, Gedevanishvili S. Full Sintering of powdered-metal bodies in a microwave field. Nature 1999;399: 668–70.

[8] Oghbaei M, Mirzaee O. Microwave versus conventional sintering: a review of fundamentals, advantages and applications. Journal of Alloys and Compounds 2010;494:175–89.

[9] Demirskyi D, Ragulya A, Agrawal D. Initial stage sintering of binderless tungsten carbide powder under microwave radiation. Ceramics International 2011;37: 505–12.

[10] Demirskyi D, Borodianska H, Agrawal D, Ragulya A, Sakka Y, Vasylkiv O. Peculiarities of the neck growth process during initial stage of spark-plasma, microwave and conventional sintering of WC spheres. Journal of Alloys and Compounds 2012;523: 1–10.

[11] Plapcianu C, Agostino A, Badica P, Aldica GV, Bonometti E, Ieluzzi G, Popa S, Truccato M, Cagliero S, Sakka Y, Vasylkiv O, Vidu R. Microwave synthesis of fullerene-doped MgB_2. Industrial and Engineering Chemistry Research 2012;51: 11005–10.

[12] Borrell A, Salvador MD, Rayon E, Penaranda-Foix FL. Improvement of microstructural properties of 3Y-TZP materials by conventional and nonconventional sintering techniques. Ceramics International 2012;38: 39–43.

[13] Costa ACFM, Tortella E, Morelli MR, Kiminami RHGA. Microstructure and magnetic properties of Ni–Zn ferrites. Journal of Magnetism and Magnetic Materials 2003;256: 174–82.

[14] Phani AR, Santucci S. Evaluation of structural and mechanical properties of aluminum oxide thin films deposited by a sol–gel process: comparison of microwave to conventional anneal. Journal of Non-Crystalline Solids 2006;352: 4093–100.

[15] Zhou XB, Qiu F, Penchal Reddy M, Han YH, Lee J, Huang Q. Comparative study of conventional and microwave sintered mullite fibers: a structural study. Advances in Applied Ceramics: Structural, Functional and Bioceramics 2015;114: 139–43.

[16] Penchal Reddy M, Madhuri W, Venkata Ramana, M, Ramamanohar Reddy N, Siva Kumar KV, Murthy VRK, Ramakrishna Reddy R. Effect of sintering temperature on structural and magnetic properties of NiCuZn and MgCuZn ferrites. Journal of Magnetism and Magnetic Materials 2010;322: 281923.

[17] Praveena K, Bououdina M, Penchal Reddy M, Srinath S, Sandhya R, Sadhana K. Structural, magnetic, and electrical properties of microwave sintered Cr^{3+} doped Sr hexa ferrites. Journal of Electronic Materials 2012;44: 1–7.

[18] Gupta M, Wong WLE. Microwaves and Metals. Singapore: John Wiley & Sons; 2007.

[19] Upadhya DD, Ram Prasad. DAE-BRNS Symposium, IT-03, 9. Shivaji University, Kolhapur.

[20] Jin Q. Microwave Chemistry. Beijing: China Science Press; 1999.

[21] Berteaud AJ, Badet JC. High temperature microwave heating in refractory materials. Journal of Microwave Power Electromagnetic Energy 1976;11: 315–20.

[22] Liu P, Wang H, Cheng X, Shui A, Zeng L. China Ceramics 2005;41(4): 12–15.

[23] Kimura T, Goto T, Shintani H, Ishizaka K, Arima T, Tokura Y, Magnetic control of ferroelectric polarization. Nature 2004;26: 55–58.

[24] Ishiwata S, Tokunaga Y, Taguchi Y, Tokura Y. High-pressure hydrothermal crystal growth and multiferroic properties of a perovskite $YMnO_3$. Journal of American Chemical Society 2011;133: 13818–13820.

[25] Chai YS, Oh YS, Wang LJ, Manivannan N, Feng SM, Yang YS, Yan YQ, Jin CQ, Kim KH. Intrinsic ferroelectric polarizations of orthorhombic manganites with E-type spin order. Physical Review B 2012;85: 184406.

[26] Lee JH, Jeong YK, Park JH, Oak MA, Jang HM, Son JY, Scott JF. Spin-canting-induced improper ferroelectricity and spontaneous magnetization reversal in $SmFeO_3$. Physical Review Letters 2011;107: 117201.

[27] Weber MC, Kreisel J, Thomas PA, Newton M, Sardar K, Walton RI. Phonon Raman scattering of $RCrO_3$ perovskites (R=Y, La, Pr, Sm, Gd, Dy, Ho, Yb, Lu). Physical Review B 2012;85: 054303.

[28] Retuerto M, Lope MJM, Hernandez GM, Munoz A, Diaz MTF, Alonso JA. Crystal and magnetic study of the disordered perovskites $Ca(Mn_{0.5}Sb_{0.5})O_3$ and $Ca(Fe_{0.5}Sb_{0.5})O_3$. Materials Research Bulletin 2010; 45: 1449–1454.

[29] Ivanov SA, Nordblad P, Tellgren R, Hewat A, Temperature evolution of structure and magnetic properties in the perovskite Sr_2MnSbO_6. Materials Research Bulletin 2009;44: 822–830.

[30] Lufaso MW, Barnes PW, Woodward PW. Structure prediction of ordered and disordered multiple octahedral cation perovskites using SPuDS. Acta Crystallographica Section B: Structural Science 2006;62: 397–410.

[31] Zhao S, Shi L, Zhou S, Zhao J, Yang H, Guo Y. Journal of Applied Physics 2009;106:123901.

[32] Wu ZY, Ma CB, Tang XG, Li R, Liu QX, Chen BT, Double-perovskite magnetic La_2NiMnO_6 nanoparticles for adsorption of bovine serum albumin applications. Nanoscale Research Letters 2013;8: 207–211.

[33] Li C, Liu B, He Y, Lv C, He H and Y. Xu. Preparation, characterization and dielectric tunability of La_2NiMnO_6 ceramics. Journal of Alloys and Compounds 2014;590: 541–545.

[34] Kumar P, Ghara S, Rajeswaran B, Muthu DVS, Sundaresan A, Sood AK. Temperature dependent magnetic, dielectric and Raman studies of partially disordered La_2NiMnO_6. Solid State Communications 2014;184: 47–51.

[35] Lin YQ, Chen XM. Local structure evolution in Ba-substituted $Pb(Fe_{1/2}Nb_{1/2})O_3$ ceramics. Journal of American Society 2011;94(3): 782–787.

[36] Murthy JK, Chandrasekhar KD, Murugavel S, Venimadhav A. Investigation of intrinsic magnetodielectric effect in La_2CoMnO_6: role of magnetic disorder. Journal of Material Chemistry C 2015; 3, 836–843.

[37] Mao Y, Facile molten-salt synthesis of double perovskite La_2BMnO_6 nanoparticles. RSC Advances 2012;2: 12675–12678.

[38] Mao Y, Parsons J, McCloy JS. Magnetic properties of double perovskite La_2BMnO_6 (B=Ni or Co) nanoparticles. Nanoscale 2013;5: 4720–4728.

[39] Zhu M, Lin Y, Lo EWC, Wang Q, Zhao Z, Xie W. Electronic and magnetic properties of La_2NiMnO_6 and La_2CoMnO_6 with cationic ordering. Applied Physics Letters 2012;100: 062406.

[40] Barrozo P, Moreno NO, Aguiar JA. Ferromagnetic cluster on La_2FeMnO_6. Advanced Materials Research 2014;975: 122–127.

[41] Qian Y, Wu H, Kan E, Lu J, Lu R, Liu Y, Tan W, Xiao C, Deng K. Biaxial strain effect on the electronic and magnetic phase transitions in double perovskite La_2FeMnO_6: a first-principles study. Journal of Applied Physics 2013;114: 063713.

[42] Rogado NS, Li J, Sleight AW, Subramanian MA. Magnetocapacitance and magnetoresistance near room temperature in a ferromagnetic semiconductor:La_2NiMnO_6. Advanced Materials 2005;17: 2225–2227.

[43] Lufaso MW, Woodward PM. Jahn–Teller distortions, cation ordering and octahedral tilting in perovskites. Acta Crystallographica Section B: Structural Science 2004;60: 10–20.

[44] Dass RI, Goodenough JB. Multiple magnetic phases of La_2CoMnO_6. Physical Review B 2003;67: 014401.

[45] Wolf SA, Awschalom DD, Buhrman RA, Daughton JM, Molnar S, Roukes ML, Chtchelkanova AY, Treger DM. Spintronics: a spin-based electronics vision for the future. Science 2001;294:1484–88.

[46] Awschalom DD, Flatte ME, Samarth N. Scientific American. 2002, 286, 66–73.

[47] Prasatkhetragarn A, Kaowphong S, Yimnirun R. Synthesis, structural and electrical properties of double perovskite Sr_2NiMoO_6 ceramics. Applied Physics A: Materials Science and Processing 2012;107(1): 117–121.

[48] Gu Y, Wang Y, Wang T, Shi W. Structure and current-induced effect on the resistivity of La_2CoMnO_6 thin films. Materials Chemistry and Physics 2012;132: 466–70.

[49] Agrawal D. Microwave sintering of ceramics, composite, metals, and transparent materials. Journal of Material Education 1999;19: 49–58.

[50] Agrawal DK, Microwave processing of ceramics: a review. Current Opinion in Solid State Material Science 1998;3: 480–486.

[51] Penchal Reddy M, Madhuri W, Ramamanohar Reddy N, Siva Kumar KV, Murthy VRK, Ramakrishna Reddy R. Influence of copper substitution on magnetic and electrical properties of MgCuZn ferrite prepared by microwave sintering method. Materials Science and Engineering: C 2010;30: 1094–1099.

[52] Uvarov U, Popov I. Metrological characterization of X-ray diffraction methods for nanocrystallite size determination. Material Characterization 2007;58: 883–91.

[53] Carron LM, Andres A, Lopez MJM, Casais MT, Alonso JA. Raman phonons as a probe of disorder, fluctuations, and local structure in doped and undoped orthorhombic and rhombohedral manganites. Physical Review B 2002;66: 174303.

[54] Carron LM, Andres A. Excitations of the orbital order in $RnMnO_3$ manganites: light scattering experiments. Physical Review Letters 2004;92: 175501.

[55] Guo H, Burgess J, Street S, Gupta A, Calvarese TG, Subramanian MA. Structural and magnetic properties of epitaxial thin films of the ordered double perovskite La_2CoMnO_6. Applied Physics Letters 2006;89: 022509.

[56] Burgess J, Guo H, Gupta A, Street S. Raman spectroscopy of La_2NiMnO_6 films on $SrTiO_3$ (100) and $LaAlO_3$ (100) substrates: observation of epitaxial strain. Vibrational Spectroscopy 2008;48: 113–117.

[57] Kim KJ, Lee HJ, Park. Cationic behavior and the related magnetic and magnetotransport properties of manganese ferrite thin films. Journal of Magnetism and Magnetic Materials 2009;321: 3706–3711.

[58] Zhou G, Lee DK, Kim YH, Kim CW, Kang YS. Preparation and spectroscopic characterization of Ilmenite-Type $CoTiO_3$ nanoparticles. Bulletin of Korean Chemical Society 2006;27: 368–372.

[59] Schnorr JM, Swager TM. Emerging applications of carbon nanotubes. Chemical Materials 2011;23: 646–657.

[60] Zhang Z, Jian H, Tang X, Yang J, Zhu X, Sun Y. Synthesis and characterization of ordered and disordered polycrystalline La_2NiMnO_6 thin films by sol–gel. Dalton Transaction 2012;41: 11836–11840.

[61] Qing TY, Meng Y, Mei HY. Structure and colossal dielectric permittivity of Ca_2TiCrO_6 ceramics. Journal of Physics D: Applied Physics 2013;46: 015303.

[62] Liu F, Li J, Li Q, Wang Y, Zhao X, Hu Y, Wang C, Liu X. High pressure synthesis, structure, and multiferroic properties of two perovskite compounds Y_2FeMnO_6 and Y_2CrMnO_6. Dalton Transaction 2014;43: 1691–1698.

[63] Subramanian MA, Li D, Duan N, Reisner BA, Sleight AW. High dielectric constant in $ACu_3Ti_4O_{12}$ and $ACu_3Ti_3FeO_{12}$ phases. Journal of Solid State Chemistry 2000;151: 323–325.

[64] Singh AK, Goel TC, Mendiratta RG., Thakur OP, Prakash C. Dielectric properties of Mn-substituted Ni–Zn ferrites. Journal of Applied Physics 2002;91: 6626–6630.

[65] Singh AK, Choudhary RNP. Structural, dielectric and electrical properties of $Pb_{5-x}La_{1+x}Ti_{3+x}Nb_{7-x}O_{30}$ (x = 0, 1 and 2) ceramics. Journal of Physics and Chemistry of Solids, 2003;64: 1185–1193.

IntechOpen